

Electronic structure, magnetism, and spin-dependent transport of CeMnNi₄

Elena N. Voloshina,¹ Yuri S. Dedkov,^{2,*} Manuel Richter,³ and Peter Zahn^{4,†}

¹Max-Planck-Institut für Physik komplexer Systeme, Nöthnitzer Strasse 38, 01187 Dresden, Germany

²Institut für Festkörperphysik, Technische Universität Dresden, 01062 Dresden, Germany

³IFW Dresden e.V., P. O. Box 270 116, 01171 Dresden, Germany

⁴Fachbereich Physik, Martin-Luther-Universität Halle-Wittenberg, 06099 Halle/Saale, Germany

(Received 25 November 2005; revised manuscript received 17 January 2006; published 10 April 2006)

Theoretical investigations of the electronic band structure and ferromagnetism of CeMnNi₄ have been performed by means of a local spin density approximation approach. The calculated magnetic moment of $4.88\mu_B$ per formula unit is in good agreement with the value determined experimentally. Recent point-contact Andreev reflection experiments show that this compound has a relatively large transport spin polarization. The calculations reveal a much smaller polarization of the density of states and transport coefficients at the Fermi level. A shift of the Fermi level by 0.1 eV raises the polarization values close to the experimental ones.

DOI: [10.1103/PhysRevB.73.144412](https://doi.org/10.1103/PhysRevB.73.144412)

PACS number(s): 71.20.-b, 71.18.+y, 72.25.-b, 75.50.Cc

Controlling the spin of electrons within a device can produce surprising and substantial changes in its properties. A new generation of devices based upon manipulation of spins in solids may have entirely new functionality that could provide a foundation for totally new computational paradigms. Crucial to all spintronic devices are materials with a high spin polarization at the Fermi level (E_F). Ordinary metals, such as copper, have zero spin polarization, whereas ferromagnetic metals, such as iron, have spin polarization of about 40% or less at E_F . The ultimate spin-polarized materials attainable are the so-called half-metallic ferromagnets (HMFs) which have the extreme limit of spin asymmetry.¹ In these materials the band structure splitting is such that only one spin channel has available states at the Fermi surface and hence all current must be carried by electrons with parallel spin. By definition, such materials are 100% spin polarized. Practical examples include chromium dioxide (CrO₂),^{2,3} lanthanum strontium manganite (La_{0.7}Sr_{0.3}MnO₃),^{4,5} and some Heusler alloys.⁶ In reality, obtaining half-metallic spin-electronic behavior is fraught with problems mainly due to the interfaces. Conversely, some materials whose bulk electrical conduction deploys both spin channels may, due to hybridization, form half-metallic interfaces with other materials. Besides the spin polarization of the ferromagnetic material there are other factors that are crucial for the aim of spin injection. Among them the more important are (i) Fermi velocity mismatch between the source of spin-polarized electrons and the collector, (ii) difficulties in thin film preparation, and (iii) imperfections on the surface and in the bulk of HMF material.

Recently, some intriguing properties of CeMnNi₄, a ferromagnetic material with a high total magnetic moment of $4.95\mu_B$ /f. u., were discovered.⁷ As was experimentally found this material has a relatively large Curie temperature of $T_C \sim 150$ K and exhibits a large transport degree of spin polarization⁸ (DSP) of about 66% determined by the point-contact Andreev reflection (PCAR) method.⁹⁻¹¹ This fact allows one to speculate (or suggest) that this material is a HMF or close to this state.

In the present work we performed local spin density approximation (LSDA) calculations of electronic band struc-

ture and magnetic properties of CeMnNi₄. Assuming a collinear ferromagnetic ground state, the magnetic moment was determined to be about $4.88\mu_B$ /f. u. and mainly carried by Mn 3d states. In contradiction to the experimental result and suggestion that this material is a HMF or close to this state, we found a rather low spin polarization at E_F of about -20%. The ordinary and transport spin polarization of CeMnNi₄ is subsequently discussed.

To obtain accurate total energies and detailed spin-resolved electronic structure information, the full-potential local orbital (FPLO) calculation scheme was applied.¹² In the scalar-relativistic calculations the LSDA exchange and correlation potential of Perdew and Wang¹³ was used. As the basis set, Ce (4f, 5s, 5p, 5d, 6s, 6p), Mn (3s, 3p, 3d, 4s, 4p), and Ni (3s, 3p, 3d, 4s, 4p) states were employed. The lower-lying states were treated fully relativistically as core states. The treatment of the Ce 5s, 5p, Ni 3s, 3p, and Mn 3s, 3p semicorelike states as valence states was necessary to account for non-negligible core-core overlaps. The spatial extension of the basis orbitals was optimized to minimize the total energy. A \mathbf{k} mesh of 735 points in the irreducible part of the Brillouin zone (13 824 in the full zone) was used to ensure accurate density of states and band structure information, especially in the region close to the Fermi level.

Hexagonal CeNi₅ (space group $P6/mmm$) [Fig. 1(a)] may be considered as a parent compound for CeMnNi₄ (space group $F\bar{4}3m$) [Fig. 1(b)]. The latter crystallizes in the face-centered cubic AuBe₅ structure with lattice constant $a=6.957$ Å and with the following Wyckoff positions: Ce (0, 0, 0), Mn (1/4, 1/4, 1/4), and Ni (5/8, 5/8, 5/8).¹⁴ In order to determine the equilibrium lattice constant a fourth-order polynomial fit of the calculated total energy vs lattice constant dependence was performed. The LSDA lattice constant of 6.817 Å is by 2.5% smaller than the experimental one of 6.987 Å.⁷ Note that the latter value is about 0.5% larger than the earlier tabulated experimental value;¹⁴ this disagreement could point to difficulties in sample preparation.

In experimental work⁷ the magnetization versus temperature, $M(T)$, for the CeMnNi₄ sample was obtained and it reveals a sharp ferromagnetic transition with $T_C \sim 150$ K.

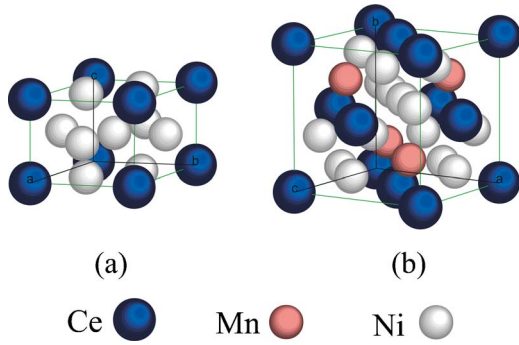


FIG. 1. (Color online) Crystallographic structures of (a) the hexagonal CeNi₅ and (b) the cubic CeMnNi₄ compound.

The signature of the ferromagnetic transition was also seen as a pronounced knee in the resistivity vs temperature, $\rho(T)$, at the same temperature. From a magnetization vs field, $M(H)$, scan recorded at 5 K a saturation magnetization of $4.95\mu_B/f.u.$ was obtained. While, in principle, in this compound all constituents (Ce, Ni, and Mn) may possess magnetic moments, the parent compound CeNi₅ is a Pauli paramagnet.¹⁵ Therefore, one can assume that the ferromagnetic transition arises due to the ordering of the Mn moments. To verify this assumption we have calculated the total magnetic moment in dependence on the lattice constant together with the site-projected moments (Fig. 2). The calculated total magnetic moment of $4.88\mu_B/f.u.$ at $a=6.817 \text{ \AA}$ is in good agreement with the experimental value. The theoretical value of the Mn magnetic moment is determined to be $3.92\mu_B/f.u.$ and $4.04\mu_B/f.u.$ for theoretical and experimental values of lattice constant, respectively. The rest of the magnetic moment is mainly due to the four Ni atoms, which together give $1.1\mu_B/f.u.$, supplemented by a small contribution of antiferromagnetically polarized Ce ($-0.14\mu_B/f.u.$).

Since hexagonal CeNi₅ can be considered as a parent compound for CeMnNi₄, we calculate the total and partial

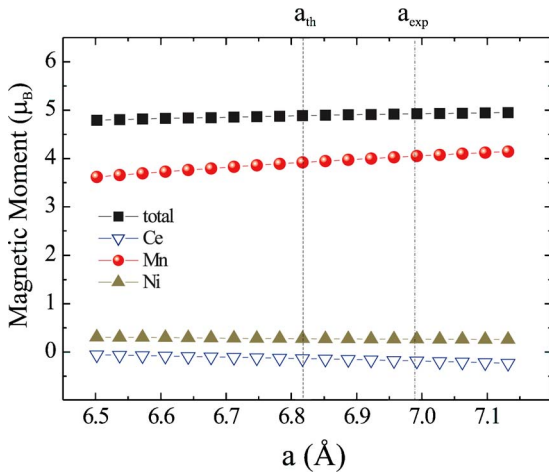


FIG. 2. (Color online) Total magnetic moment (black squares) as well as magnetic moments of Ce (open down triangles), Mn (solid circles), and Ni (solid up triangles) as a function of lattice constant of CeMnNi₄. The vertical lines mark theoretical and experimental values of the lattice constant, respectively.

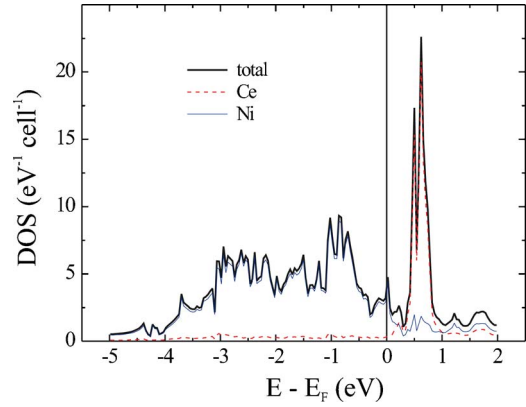


FIG. 3. (Color online) Total and partial densities of states of the nonmagnetic hexagonal CeNi₅.

densities of states (DOS and PDOS, respectively) for Ce and Ni in the former compound. The results shown in Fig. 3 are in agreement with previous calculations.¹⁵ As shown, the Stoner criterion for an instability toward ferromagnetism in this compound is not satisfied, in agreement with the fact that no magnetic ordering has been observed ($IN \approx 0.75 < 1$, where I is the Stoner integral and N is the DOS per spin at the Fermi energy).

Figures 4 and 5 show total and partial DOSs and the spin-resolved electronic band structure of CeMnNi₄ at the LSDA lattice constant, respectively. The Ce $4f$ states are situated approximately 1 eV above the Fermi level and they are weakly polarized. Ni (mostly $3d$) states are also weakly polarized, but in the opposite way. Mn (mainly $3d$) occupied

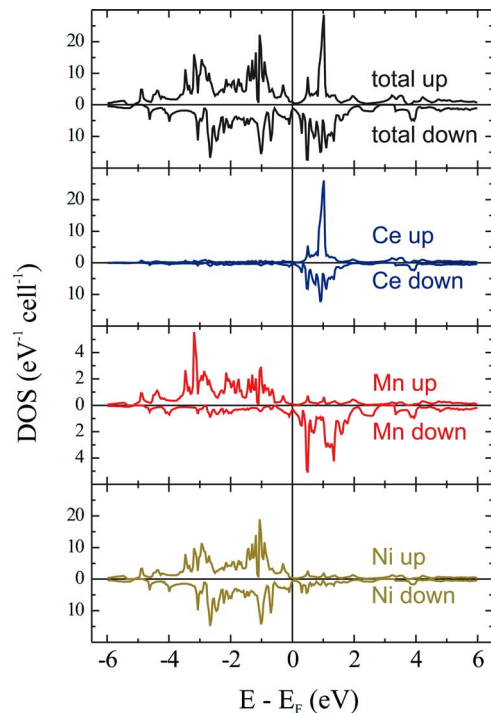


FIG. 4. (Color online) Total spin-dependent DOS of CeMnNi₄ and the local DOS for Ce, Mn, and Ni (from top to bottom), respectively.

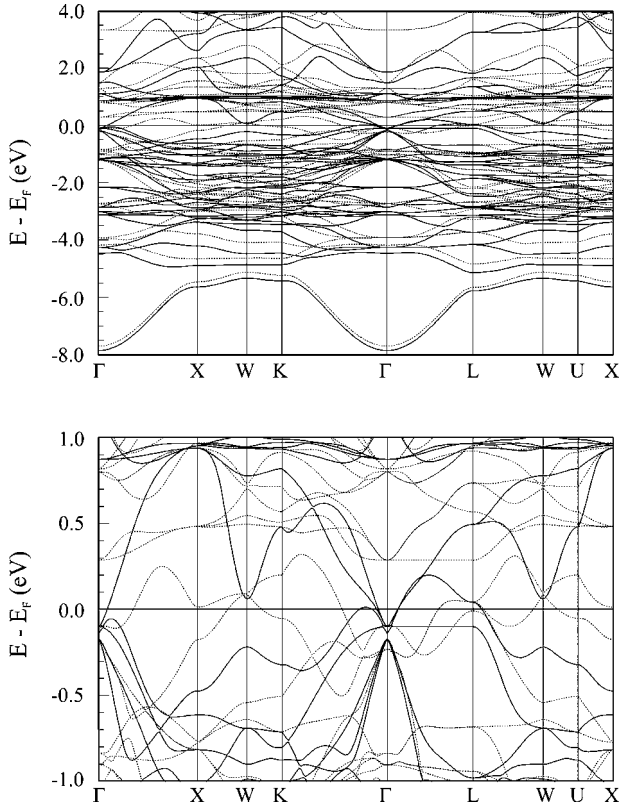


FIG. 5. The spin-resolved band structure of CeMnNi_4 over wide energy range (upper panel) and in the vicinity of Fermi level (lower panel). Solid and broken lines represent spin-up and spin-down electronic channels, respectively.

states are found in the region between 0.5 and 3.5 eV below E_F . It is remarkable that the Mn 3d bandwidth in the majority-spin channel is much larger (about 3 eV) than in the minority one (about 1.5 eV). This disparity arises from different interaction partners available in the two spin channels. Majority-spin Mn 3d states are hybridized with the almost fully occupied Ni 3d states that form a band of about the same width as in elemental Ni metal, due to the large Ni concentration. On the other hand, the minority-spin Mn 3d states are split off due to exchange interaction by more than 3 eV. Thus, they hybridize with the Ce 4f states that are available at this energy, around 1 eV above Fermi level, and form a narrow band due to the small number of neighbors at slightly larger interatomic distance (four Mn-Ce neighbors at 3.01 Å compared with 12 Mn-Ni neighbors at 2.88 Å). The described band structure explains the position of the Fermi level in a valley of the DOS: the Ni 3d band is virtually filled and the Mn 3d band is split into a filled spin-up band and an empty spin-down band. What remains at the Fermi level are broad *sp* (and Ce 5d) bands.

The corresponding densities of states at E_F for spin-up and spin-down channels in CeMnNi_4 are $N_{\uparrow} = 0.96 \text{ eV}^{-1} \text{ f.u.}^{-1}$ and $N_{\downarrow} = 1.54 \text{ eV}^{-1} \text{ f.u.}^{-1}$ giving an electronic specific heat coefficient γ of $5.8 \text{ mJ mol}^{-1} \text{ K}^{-2}$. Though the Fermi level is situated in a DOS valley, the DOS at E_F is comparable to values found in normal metals like Al (about $0.3 \text{ eV}^{-1} \text{ atom}^{-1}$), and to the value found, e.g., in HMF CrO_2 ($N_{\uparrow} \approx 1.9 \text{ eV}^{-1} \text{ f.u.}^{-1}$).¹⁶

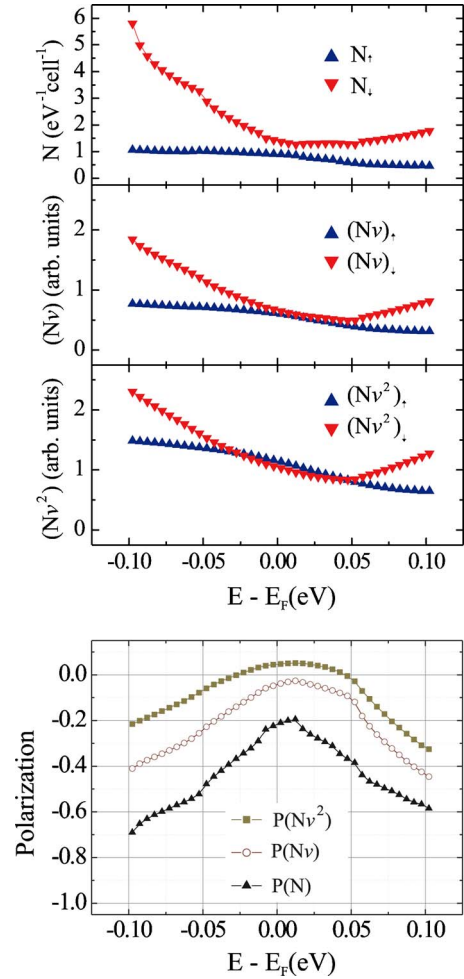


FIG. 6. (Color online) Spin-dependent densities of states N , Sharvin conductance (Nv) , plasma frequencies (Nv^2) (upper panel), and the derived spin polarizations (lower panel) at the theoretical lattice constant of CeMnNi_4 .

The calculated spin polarization of the DOS at E_F , $P(N) = (N_{\uparrow} - N_{\downarrow}) / (N_{\uparrow} + N_{\downarrow})$, of CeMnNi_4 amounts to -16% and -21% in case of experimentally determined and LSDA lattice constants, respectively. These values are substantially lower than the experimentally determined polarization of 66% .⁷ This discrepancy may originate from two sources that we will discuss subsequently: (i) oversimplified analysis of the experimental data and/or (ii) off-stoichiometry of the sample.

As it was previously pointed out by Mazin⁸ the DSP for Andreev reflection can be interpreted in terms of spin-dependent transport coefficients $(Nv)^{\uparrow,\downarrow}$ and $(Nv^2)^{\uparrow,\downarrow}$ for the limits of ballistic and diffusive transport, respectively, neglecting the state-dependent transmittance of the barrier between normal metal and superconductor. They correspond to the Sharvin conductance and the plasma frequency squared, respectively, and are given by Fermi surface integrals over Fermi velocities $v_{\mathbf{k}}$: $(Nv)^{\uparrow,\downarrow} \propto \int d^3\mathbf{k} \delta(E_{\mathbf{k}}^{\uparrow,\downarrow} - E_F) v_{\mathbf{k}}^{\uparrow,\downarrow}$ and $(Nv^2)^{\uparrow,\downarrow} \propto \int d^3\mathbf{k} \delta(E_{\mathbf{k}}^{\uparrow,\downarrow} - E_F) (v_{\mathbf{k}}^{\uparrow,\downarrow})^2$. The behavior of the spin-dependent quantities N , (Nv) , and (Nv^2) is given for the theoretical lattice constant in Fig. 6 (upper panel) for energies around the Fermi level. At the Fermi level the obtained

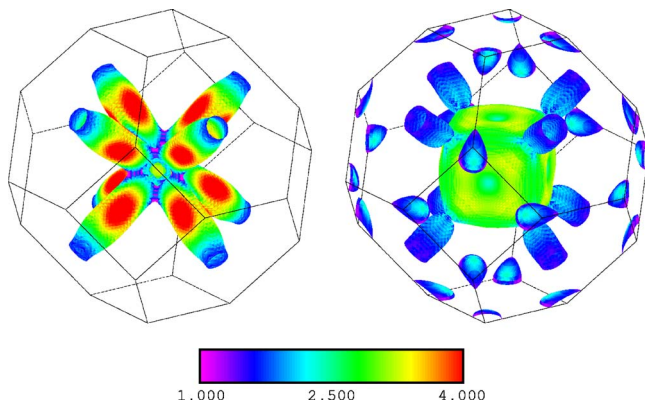


FIG. 7. (Color online) Fermi velocity distribution $|v_{\mathbf{k}}|$ for majority (left) and minority (right) spin states of CeMnNi_4 at the theoretical lattice constant (in units of $8.1 \times 10^6 \text{ cm sec}^{-1}$).

polarizations [Fig. 6 (lower panel)] are substantially smaller than in experiment, but for changes of the Fermi level by approximately 0.1 eV, values close to the experimentally ones are reached. The effect is most pronounced for N , and is weaker for $(N\nu)$ and $(N\nu^2)$ because the spin asymmetry of the Fermi velocity is opposite to the spin asymmetry of the DOS. Possible discrepancies of the polarizations derived from PCAR measurements using a Blonder-Tinkham-Klapwijk (BTK) scheme¹⁷ and derived from bulk electronic structure are elucidated by Xia *et al.*¹⁸ The BTK approach uses very simplified model barriers and in the analysis of the experimental data parabolic electronic bands were employed.⁷ In real tunneling experiments a large part of the current is carried by few electronic states of high transmission [compare Fig. 1d in Ref. 18]. From the spin-dependent Fermi velocities shown in Fig. 7 it is evident that this selection may change the apparent spin polarization of the ferromagnet drastically. The highly conducting majority states (left panel, states on the tubes along the Γ -L direction and close to the Γ point) may cause an opposite spin polarization of current than the polarization of the DOS. So the interpre-

tation of Andreev reflection measurements in terms of bulk polarizations can be highly misleading. In addition, interface effects may render the BTK analysis invalid.

Another reason for the discrepancy of experimental results and theoretical values at the Fermi level could be given by stoichiometric variations of the sample. A change of the Fermi level's position by about 0.1 eV can lead to a drastic change of the DOS spin polarization up to approximately -70% . Such a shift would occur, e.g., if 5% of Mn is replaced by Ni during the preparation process. This knowledge can be used in future sample optimization to increase spin polarization by controlled alloying of CeMnNi_4 .

A recently published work by Mazin¹⁹ considers the electronic structure and Fermi surface properties of cubic CeMnNi_4 in the generalized gradient approximation (GGA) of density functional theory. While our results on the DOS, the Fermi surface topology, and the plasma frequency agree very well with his results, there are small differences visible in the band structures, which might be related to the different approximations (LSDA vs GGA) used.

In conclusion, the spin-resolved electronic band structure, magnetic properties, and transport coefficients of CeMnNi_4 , a recently investigated soft magnetic material with high transport spin polarization and high magnetic moment, were studied. The theoretically calculated value of magnetic moment is in good agreement with experiment. In contrast to the high transport spin polarization derived from point-contact Andreev reflection, the calculated values for the bulk material are low. We suggest two possible reasons for this discrepancy: (i) oversimplified analysis of the experimental data in terms of model barriers and parabolic bands and (ii) possible small off-stoichiometry of the sample shifting the position of the Fermi level. We propose to study the influence of well-controlled off-stoichiometry on the transport spin polarization of CeMnNi_4 .

This work has been supported by the DFG through SFB 463.

*Email address: dedkov@physik.phy.tu-dresden.de

†Also at Institut für Theoretische Physik, Technische Universität Dresden, 01062 Dresden, Germany.

¹W. E. Pickett and J. S. Moodera, *Phys. Today* **54** (5), 39 (2001).

²K.-H. Schwarz, *J. Phys. F: Met. Phys.* **16**, L211 (1986).

³M. A. Korotin, V. I. Anisimov, D. I. Khomskii, and G. A. Sawatzky, *Phys. Rev. Lett.* **80**, 4305 (1998).

⁴W. E. Pickett and D. J. Singh, *Phys. Rev. B* **53**, 1146 (1996).

⁵P. K. de Boer, H. van Lenken, R. A. de Groot, T. Rojo, and G. E. Barberis, *Solid State Commun.* **102**, 621 (1997).

⁶R. A. de Groot, F. M. Mueller, P. G. van Engen, and K. H. J. Buschow, *Phys. Rev. Lett.* **50**, 2024 (1983).

⁷S. Singh, G. Sheet, P. Raychaudhuri, and S. K. Dhar, *Appl. Phys. Lett.* **88**, 022506 (2005).

⁸I. I. Mazin, *Phys. Rev. Lett.* **83**, 1427 (1999).

⁹A. F. Andreev, *Zh. Eksp. Teor. Fiz.* **46**, 1823 (1964); [*Sov. Phys. JETP* **19**, 1228 (1964)].

¹⁰R. J. Soulen, Jr., J. M. Byers, M. S. Osofsky, B. Nadgorny *et al.*, *Science* **282**, 85 (1998).

¹¹S. K. Upadhyay, A. Palanisami, R. N. Louie, and R. A. Buhrman, *Phys. Rev. Lett.* **81**, 3247 (1998).

¹²Computer code FPLO-5.00-18 [improved version of the original FPLO code by K. Koepnick and H. Eschrig, *Phys. Rev. B* **59**, 1743 (1999)], <http://www.FPLO.de>

¹³J. P. Perdew and Y. Wang, *Phys. Rev. B* **45**, 13244 (1992).

¹⁴P. Villars and L. D. Calvert, *Pearson's Handbook of Crystallographic Data for Intermetallic Phases* (American Society for Metals, Metal Park, OH, 1989), Vols. 1-3.

¹⁵L. Nordström, M. S. S. Brooks, and B. Johansson, *Phys. Rev. B* **46**, 3458 (1992).

¹⁶I. I. Mazin, D. J. Singh, and C. Ambrosch-Draxl, *Phys. Rev. B* **59**, 411 (1999).

¹⁷G. E. Blonder, M. Tinkham, and T. M. Klapwijk, *Phys. Rev. B* **25**, 4515 (1982).

¹⁸K. Xia, P. J. Kelly, G. E. W. Bauer, and I. Turek, *Phys. Rev. Lett.* **89**, 166603 (2002).

¹⁹I. I. Mazin, cond-mat/0510400; *Phys. Rev. B* **73**, 012415 (2006).